

Cite this article as: He Miaoxia, Yan Chi, Dong Yuecheng, et al. Effect of Mn Microalloying on Microstructure Evolution and Mechanical Properties of Ti-Al-Mo-Zr-Fe-B Alloy[J]. Rare Metal Materials and Engineering, 2024, 53(06): 1555-1565. DOI: 10.12442/j.issn.1002-185X.20230547.

ARTICLE

Effect of Mn Microalloying on Microstructure Evolution and Mechanical Properties of Ti-Al-Mo-Zr-Fe-B Alloy

He Miaoxia¹, Yan Chi², Dong Yuecheng¹, Chang Hui¹, Alexandrov Igor V²

¹ *Tech Institute for Advanced Materials, College of Materials Science and Engineering, Nanjing Tech University, Nanjing 211816, China;*

² *Department of Materials Science and Physics of Metals, Ufa University of Science and Technology, Ufa 450008, Russia*

Abstract: The effects of Mn microalloying on the microstructure and mechanical properties of new near- α Ti-Al-Mo-Zr-Fe-B alloy were studied by OM, EBSD, and TEM. Results indicate that the addition of 0.5wt% Mn can refine the casting microstructure of the alloy from 3.28 μm to 2.65 μm , which leads to the increase in ultimate tensile strength from 882 MPa to 966 MPa. However, the elongation decreases from 7.8% to 5.1%. After forging, the grain size of two alloys tends to be similar, and the microstructure is more equiaxed. Besides, the microstructure becomes more homogeneous after Mn microalloying. The ultimate tensile strength and elongation of Ti-Al-Mo-Zr-Fe-B alloy increase to 966 MPa and 16.4%, respectively, whereas the alloy containing 0.5wt% Mn element possesses higher ultimate tensile strength, reaching 1079 MPa. Meanwhile, the elongation reaches 15.8%. These results suggest that the increase in strength can be attributed to the solid solution strengthening effect of Mn element. Additionally, the Mn microalloying promotes the enrichment of Al element in alloy into the α phase, which is beneficial to improve the strength and plasticity of the alloy.

Key words: Mn microalloying; near- α titanium alloy; microstructure evolution; mechanical property

Titanium alloys are widely used in marine engineering, petrochemical industry, aerospace, and other fields due to their advantages of high strength, lightweight, high fatigue properties, and excellent corrosion resistance^[1-7]. In recent years, a novel submarine for diving at 10 000 m depth has been designed. The shell of submarine is made of Ti-6Al-3Mo-2Sn-2Zr-1Cr-1V (Ti62A) titanium alloy, which has a high yield strength over 950 MPa, tensile strength over 1000 MPa, and good ductility over 15%^[8-9]. However, the welding efficiency of Ti62A alloy with $\alpha + \beta$ microstructure is extremely low. Ti-6Al-3Nb-2Zr-1Mo (Ti80) alloy is a typical near- α alloy with excellent weldability^[10-11], good impact toughness^[12], low fatigue cracking performance^[13-14], and good corrosion resistance^[15], which is widely used in marine engineering and shipbuilding industry. However, the yield stress of Ti80 alloy is 800 MPa, which is not enough for the construction of innovation submarine^[16-17]. Furthermore, the refractory metal Nb in Ti80 alloy is expensive and highly refractory. A new near- α Ti-6Al-1Mo-2Zr-0.55Fe-0.1B titanium alloy has been

designed by substituting Fe and B elements for Nb element^[18], it achieves the expected tensile stress and ductility, but its yield stress is still unqualified. Hence, it is important to simultaneously enhance the yield stress and to retain the good ductility of Ti-6Al-1Mo-2Zr-0.55Fe-0.1B alloy.

Microalloying has been proved to be a simple and effective method to improve the properties of materials^[19-23]. As the eutectoid β -stabilizing element with low cost and low melting point, Mn has good strengthening effect, which is beneficial to the development of titanium alloys with low cost, high strength, and good ductility^[24-25]. Zhang et al^[26] studied the microstructure, mechanical properties, and cell proliferation properties of Ti-(2, 5, 8, 12)Mn alloys. It is found that the addition of Mn increases the hardness of pure titanium from 69.2 GPa to 122.0 GPa (Ti12Mn alloy). However, the plasticity decreases from 25.0% to 11.7%. Jawed et al^[27] found that the addition of Mn (3wt%, 5wt%) significantly refines the grains of Ti-Nb-Zr-Mn alloy. Compared with those of Ti-26Nb-3Mn-4Zr alloy, the hardness (HV) and strength of Ti-

Received date: September 03, 2023

Foundation item: National Key Research and Development Program of China (2021YFB3700802); Russian Science Foundation Project (23-43-00041); National Natural Science Foundation of China (51931008); Priority Academic Program Development of Jiangsu Higher Education Institutions (PAPD)

Corresponding author: Dong Yuecheng, Ph. D., Associate Professor, Tech Institute for Advanced Materials, College of Materials Science and Engineering, Nanjing Tech University, Nanjing 211816, P. R. China, E-mail: dongyuecheng@njtech.edu.cn

Copyright © 2024, Northwest Institute for Nonferrous Metal Research. Published by Science Press. All rights reserved.

26Nb-5Mn-4Zr alloy increase by 166.6 and 18 MPa, respectively, and the self-corrosion potential (E_{corr}) also increases from 0.45 V to 0.48 V. Liu et al.^[28] found that the high temperature strength of Ti-45Al-3Nb alloy is significantly improved by the addition of Mn, Cr, and Mo elements, and the deformation ability of Ti-45Al-3Nb ternary alloy is significantly enhanced. Obviously, the addition of Mn element has a positive effect on the microstructure and properties of titanium alloys.

Mn element has a good solid solution strengthening effect for the titanium alloys, but its influence on ductility strongly depends the alloying system^[27,29]. In this research, the effect of Mn element on the microstructure and mechanical properties of the near- α Ti-6Al-1Mo-2Zr-0.55Fe-0.1B alloy was investigated, and the strengthening and toughening mechanisms were discussed.

1 Experiment

Ingot of Ti-6Al-1Mo-2Zr- x Mn-0.55Fe-0.1B alloy with $x=0, 0.5$ (wt%) was prepared by high purity sponge titanium (99.6%), Al bean (99.9%), pure Zr (99.4%), Al-30Mn, Al-60Mo, Ti-32Fe, and Fe-25B master alloys, and the prepared alloys were denoted as 0Mn and 0.5Mn alloys, respectively. After ultrasonic cleaning, the alloys were pressed into a dense electrode block, and the ingot was remelted three times by vacuum arc remelting (VAR) equipment. The chemical composition of the alloys was determined by inductively coupled plasma-mass spectrometer (ICP-MS), and the results are shown in Table 1. According to the theoretical calculation method and metallographic method, the phase transition points of the 0Mn and 0.5Mn alloys are 995 ± 5 °C and 985 ± 5 °C, respectively.

In order to eliminate the defects caused by casting and to refine the microstructure, the 0Mn and 0.5Mn alloys were forged in three steps. Firstly, two piers and two billets were forged at 150 °C (above the phase transition point). Then, the

Table 1 Chemical composition of 0Mn and 0.5Mn alloys (wt%)

Alloy	Al	Mo	Zr	Fe	B	Mn	Ti
0Mn	5.80	1.07	1.85	0.57	0.044	0.00	Bal.
0.5Mn	5.63	0.97	1.99	0.63	0.069	0.51	Bal.

re-forging was conducted at 100 °C (above the phase transition point). The first and second heating processes ensured that the deformation amount was 60%. The final forging temperature was 50 °C (below the phase transition point), and the deformation amount was guaranteed as 80%. The specimens were air-cooled after each heating process. The flow chart of the casting and forging processes of 0Mn and 0.5Mn alloys is shown in Fig. 1. After machining, the specimens of $\Phi 100$ mm \times 100 mm and $\Phi 50$ mm \times 100 mm were cut from the effective area of ingot and forging rod, respectively. The metallographic specimens were polished step by step with sandpaper and etched by metallographic etchant with the volume ratio of HF:HNO₃:H₂O=1:2:7. The microstructure was analyzed by optical microscope (OM, Zeiss Axio Observer A1m) and Image Pro Plus image analysis software.

The quasi-static tensile specimens were processed into the standard specimens with gauge length of 28 mm and cross-sectional diameter of 5 mm according to GB/T228-2002 standard. According to GB/T 228.1-2010 standard, the uniaxial tensile tests at room temperature were conducted by Instron 4507 universal testing machine^[30]. The YYU-10/25 type extensometer was used, the axial tensile rate was 1 mm/min, and the strain rate was 7×10^{-3} s⁻¹. The specimens at different states were subjected to three repeated tests. The hardness of the alloys was tested by HV-1000 microhardness tester.

The microstructure and element distribution of the alloy were characterized by X'TRA X-ray diffractometer (XRD), FEI Tena G2 F30 transmission electron microscope (TEM), and electron backscattered diffraction (EBSD). XRD tests

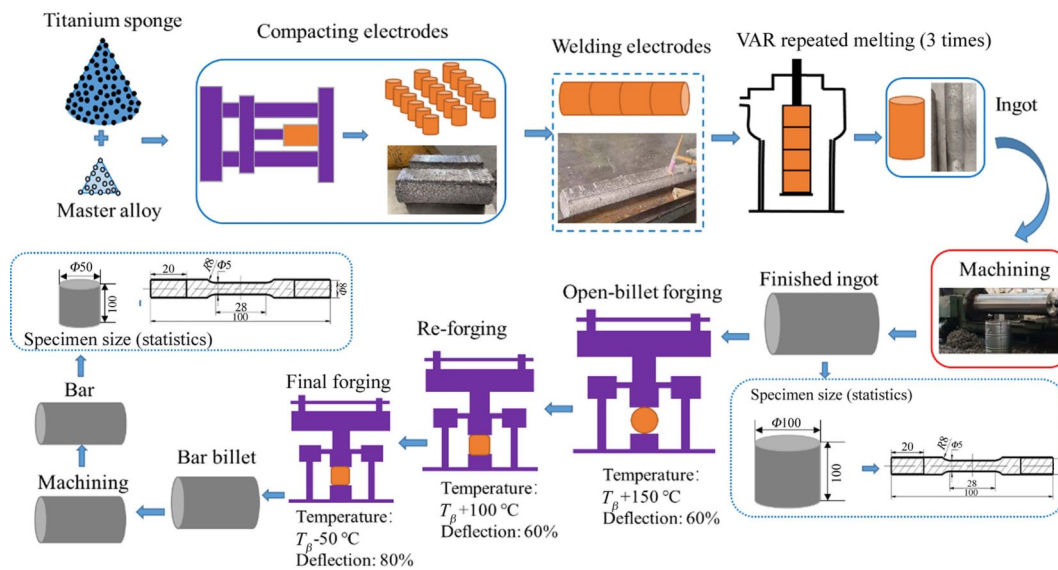


Fig.1 Flow chart of casting and forging processes of 0Mn and 0.5Mn alloys

were performed using Cu target $K\alpha_1$ at the wavelength of 0.154 18 nm, scanning speed of $10^\circ/\text{min}$, and scanning angle of $2\theta=20^\circ-90^\circ$. The fracture morphologies of specimens after tensile tests were characterized by Hitachi Regulus 8100 cold field emission scanning electron microscope (SEM). SEM specimens were observed at the secondary electron mode. EBSD specimen dimension was $10\text{ mm}\times 10\text{ mm}\times 5\text{ mm}$. EBSD was performed by field emission SEM (JSM-6700F) equipped with Oxford instrument EBSD detector with test voltage of 20 kV, step size of $0.05\text{ }\mu\text{m}$, and scanning area of $1600\text{ }\mu\text{m}^2$.

2 Results and Discussion

2.1 Microstructure and phase content of as-cast alloys

Fig.2 shows the microstructures and grain sizes of as-cast 0Mn and 0.5Mn alloys after air cooling. The as-cast microstructures of the two alloys are mainly composed of lamellar α phase and intergranular β phase. The lamellar α phase is interlaced with each other. The thickness of the lamellar phase of the 0Mn alloy is basically $2.5-3\text{ }\mu\text{m}$ with the average thickness around $3.28\text{ }\mu\text{m}$. After adding 0.5wt% Mn, the grain boundary α phase appears in the alloy, and the lamellar α phase is interlaced in a cluster manner. The lamellar phase thickness is basically $2-2.5\text{ }\mu\text{m}$ with the average thickness around $2.65\text{ }\mu\text{m}$. Obviously, the trace addition of Mn element can significantly refine the lamellar phase thickness of the as-cast alloy and the grain boundary becomes clearer.

Fig. 3 shows XRD patterns of as-cast 0Mn and 0.5Mn alloys. The two alloys are mainly composed of α phase with close-packed hexagonal (hcp) structure and β phase with body-centered cubic structure. The content of β phase is relatively small. After adding Mn element, the relative intensity of β phase peak of the alloy increases slightly. This indicates that

Mn enhances the stability of β phase, and more β phases are retained at room temperature. In addition, the β -Ti peak of the 0.5Mn alloy shifts to a high angle area, which is attributed to the dissolution of Mn element in the solid solution. The Mn atoms occupy the lattice sites of the original titanium atoms. Because the radius of Mn atom (0.127 nm) is smaller than that of Ti (0.147 nm)^[31], the lattice distortion occurs, the lattice constant decreases, and the diffraction angle increases. Additionally, because of the addition of B element, a weak diffraction peak of TiB phase can also be found near $2\theta=45^\circ$, and no Ti-Mn intermediate compound can be detected. Obviously, 0.5wt% Mn addition in titanium alloy cannot introduce obvious new phase formation in the alloy, but only changes the phase content slightly.

2.2 Microstructure of forged alloys

Fig.4 shows the microstructures and grain sizes of forged 0Mn and 0.5Mn alloys. The microstructure of the forged alloys is mainly composed of short rod-shaped primary α phase and intergranular β phase. After multiple plastic deformation during the forging process, the strip-shaped lamellar α phase is broken, and a small amount of equiaxed α phase appears in the local position. The lamellar structure thickness of the primary α phase is basically $3-5\text{ }\mu\text{m}$. Many elongated grains exist in the 0Mn alloy with average grain thickness of about $4.58\text{ }\mu\text{m}$. The content of β phase is only 6.7%, and the content of α phase is 93.3%.

After adding 0.5wt% Mn, more α phases in the alloy are spheroidized, and the grains in 0.5Mn alloy show good equiaxiality with average grain lamella thickness of approximately $4.25\text{ }\mu\text{m}$. Obviously, the grain size of the two forged alloys has slight difference. However, compared with that of the as-cast alloys, the microstructure distribution of the forged alloy is more uniform and orderly. It can be seen that

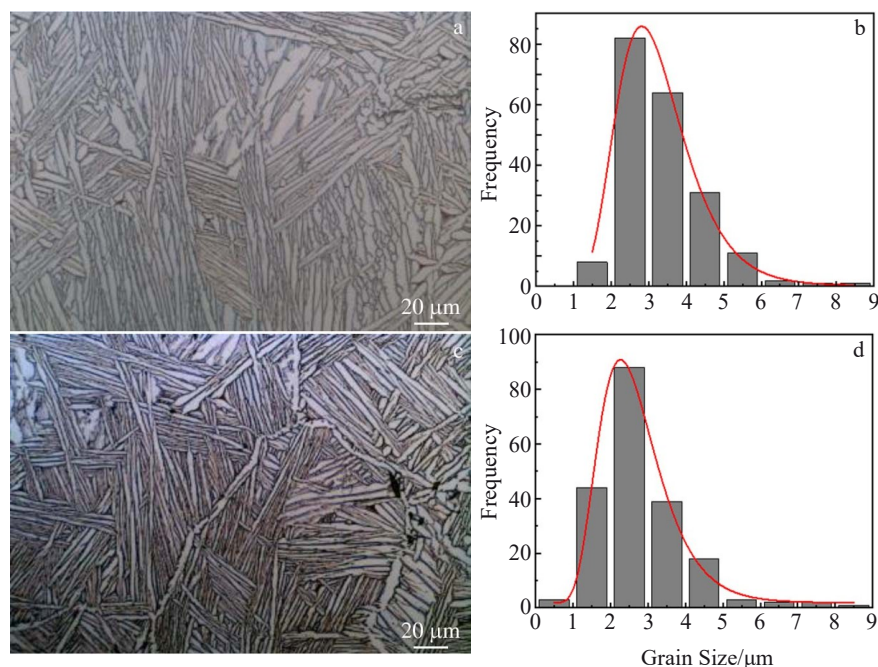


Fig.2 Microstructures (a, c) and grain sizes (b, d) of as-cast 0Mn alloy (a-b) and 0.5Mn alloy (c-d)

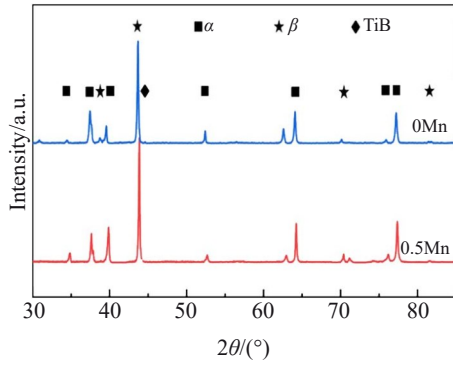


Fig.3 XRD patterns of as-cast 0Mn and 0.5Mn alloys

the trace addition of Mn element results in more equiaxed microstructure of the forged Ti-Al-Mo-Zr-Fe-B alloys.

The inverse pole figures (IPFs) of the two forged alloys are shown in Fig.5. Different colors in the diagram represent the grains with different orientations: red represents the grains parallel to the basal plane $\{0001\}$; green represents the grains parallel to the cylinder $\{\bar{1}2\bar{1}0\}$; blue represents the grains parallel to the cone $\{01\bar{1}0\}$. Other colors are the transition colors, and they represent the transition between orientation differences^[32]. The larger the color difference, the larger the orientation difference between the grains. According to IPFs in Fig.5, the microstructure distribution of the 0Mn alloy after forging is not uniform, the orientation difference is mainly based on the base surface, and the orientation difference between the grains is large. The grain size difference of 0Mn alloy after forging is large. The minimum grain size is about 2.5 μm , and the maximum is more than 8 μm . The average grain lamella thickness of the forged 0Mn alloy is 4.58 μm , which is in good agreement with the results in Fig. 4. The

microstructure distribution of forged 0.5Mn alloy is equiaxed and more uniform than that of forged 0Mn alloy. The aspect ratios of forged 0Mn and 0.5Mn alloys are about 2.0 and 1.3, as shown in Fig5c and 5f, respectively. Although the average grain lamella thickness is similar (4.25 μm), the orientation between the equiaxed α phase and the matrix is arbitrary.

Fig. 6 shows the kernel average misorientation (KAM) diagrams of the forged 0Mn and 0.5Mn alloys. KAM diagram can macroscopically represent the geometrically necessary dislocation and evaluate the strain distribution of alloys. The higher the KAM value, the higher the dislocation density in this region, and the higher the energy stored in the grains. $\text{KAM} > 0.5^\circ$ is defined as the high density dislocation (green in KAM diagram); $\text{KAM} \leq 0.5^\circ$ is defined as a low density dislocation (blue in KAM diagram). It can be seen that KAM distribution in 0.5Mn alloy is more uniform than that in 0Mn alloy. Considering the strain in the grains, the strain accumulation near the grain boundary is larger, indicating that the dislocation is more likely to aggregate at the grain boundary. The proportion of high density dislocations in forged 0Mn and 0.5Mn alloys reaches 51.8% and 45.4%, respectively. After adding Mn element, the dislocation density presents a downward trend. At the same time, the average KAM values of forged 0Mn and 0.5Mn alloys are 0.21 and 0.19, respectively. The relatively high strain in the alloy is caused by the dislocation slip and entanglement during the plastic deformation, and the phase transition strain is caused by the precipitation of α phase from the β matrix^[33].

Fig. 7 shows the grain boundary diagrams and misorientation distribution diagrams of 0Mn and 0.5Mn alloys. High angle grain boundaries (HAGBs) with misorientation angle $> 15^\circ$ are represented by the black lines, and the low angle grain boundaries (LAGBs) with misorientation angles

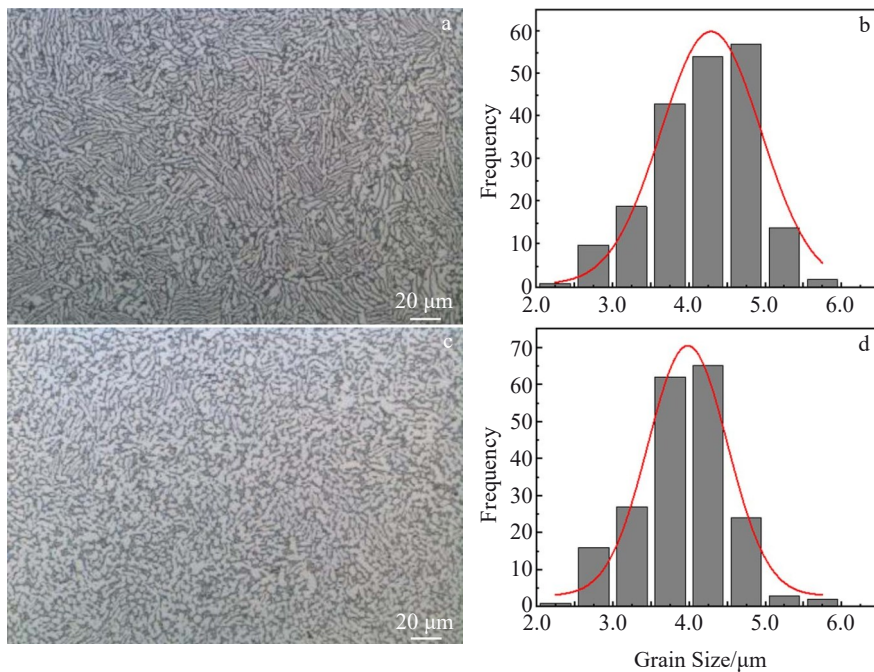


Fig.4 Microstructures (a, c) and grain sizes (b, d) of forged 0Mn alloy (a-b) and 0.5Mn alloy (c-d)

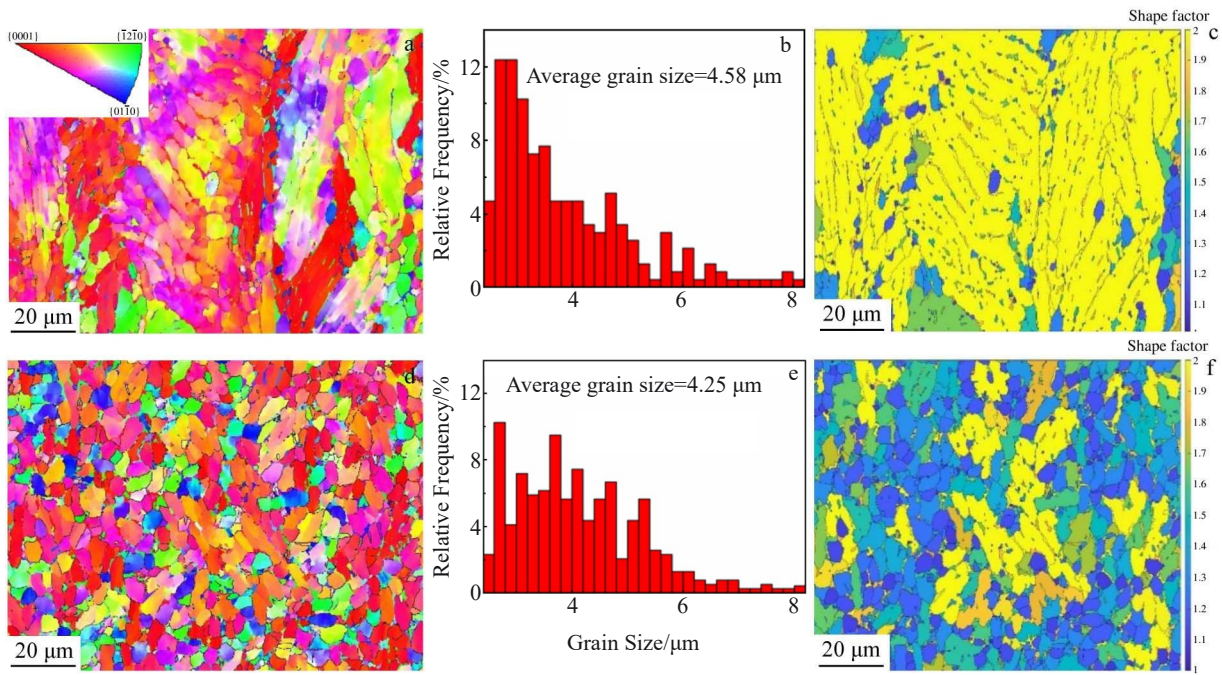


Fig.5 IPFs (a, d), grain sizes (b, e), and the ratio of length to diameter size distribution maps (c, f) of forged 0Mn alloy (a–c) and 0.5Mn alloy (d–f)

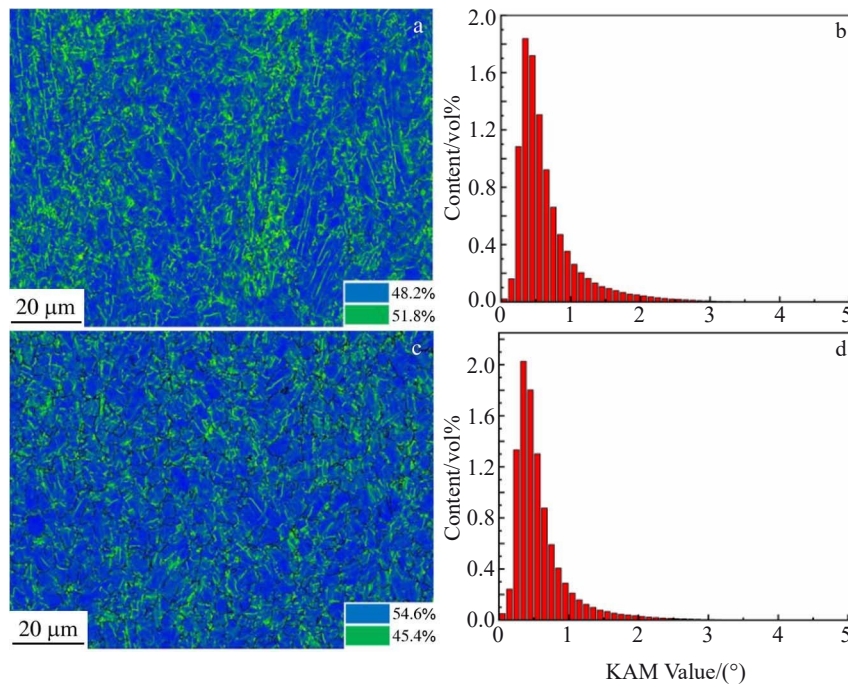


Fig.6 KAM distribution maps (a, c) and KAM results (b, d) of forged 0Mn alloy (a–b) and 0.5Mn alloy (c–d)

of 2°–15° are represented by the red lines. The proportion of red lines in the grain boundary diagram of forged 0Mn and 0.5Mn alloys is larger than that of black lines, so the grain boundary is mainly dominated by LAGBs. The analysis results show that the proportion of LAGBs in forged 0Mn and 0.5Mn alloys is 86.39% and 76.95%, respectively. The orientation difference of the two alloys shows a strong peak of orientation difference between 2° and 5°, whereas the

orientation difference around 60° and 85° shows weak peaks.

Fig. 8 shows the internal average misorientation angle (IAMA) diagrams and grain contents of forged 0Mn and 0.5Mn alloys. According to IAMA standard, the microstructures of the forged 0Mn and 0.5Mn alloys can be divided into three types: recrystallized grains, substructured grains, and deformed grains. When IAMA < 1°, it is defined as the substructured grain and represented by the yellow area. When

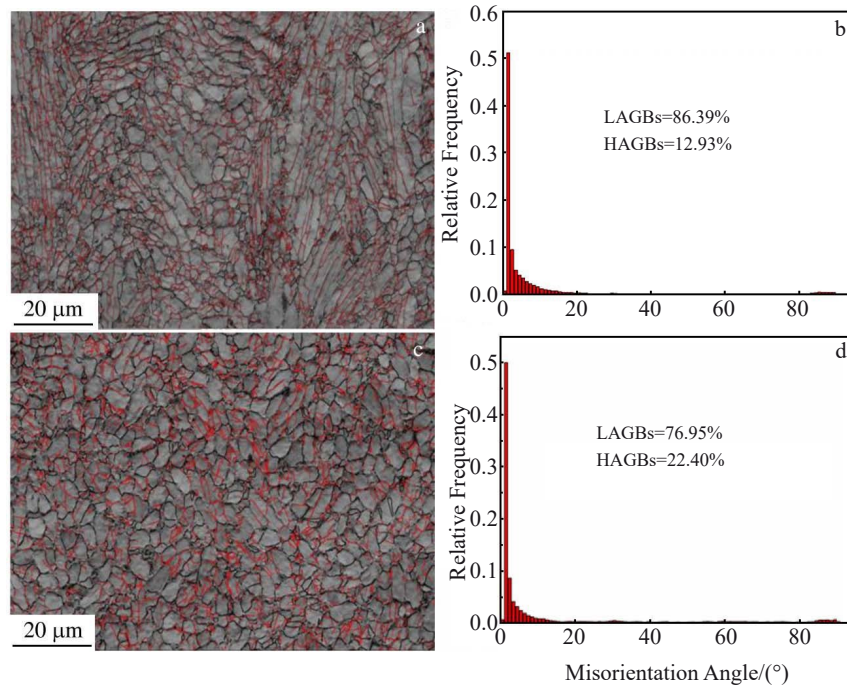


Fig.7 Grain boundary diagrams (a, c) and misorientation angle distributions (b, d) of forged 0Mn alloy (a–b) and 0.5Mn alloy (c–d)

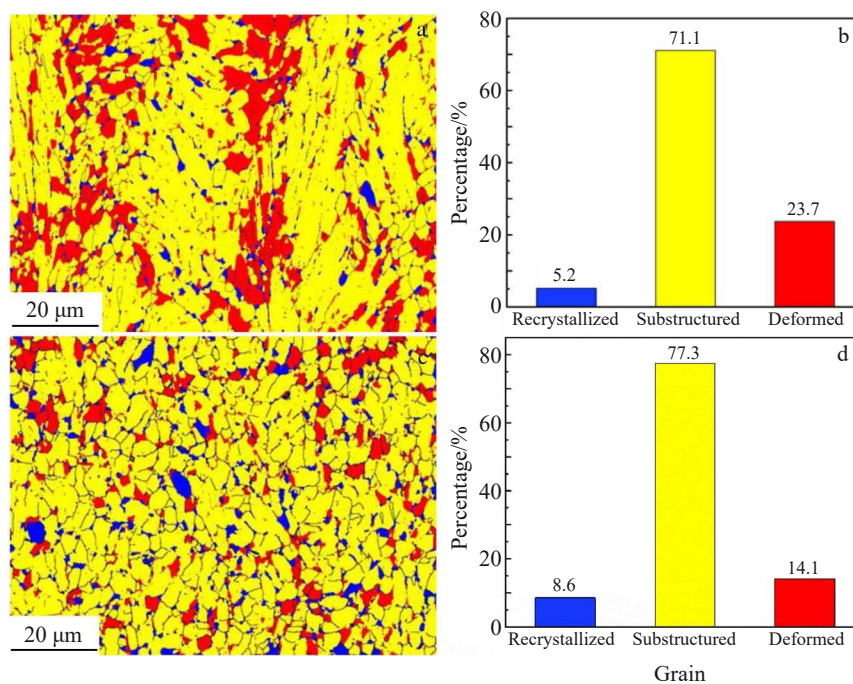


Fig.8 IAMA diagrams (a, c) and grain contents (b, d) of forged 0Mn alloy (a–b) and 0.5Mn alloy (c–d)

IAMA $>1^\circ$, it is defined as deformed grain and represented by the red area. The rest are recrystallized grains, which are represented by the blue area.

It can be seen that the majority components in forged 0Mn and 0.5Mn alloys are substructured grains, and the proportion of deformed and recrystallized grains is very small. The proportion of substructured grains reaches 71.1% and 77.3% in the forged 0Mn and 0.5Mn alloys, respectively. The

proportion of deformed grains in the forged 0Mn and 0.5Mn alloys is 23.7% and 14.1%, respectively. The proportion of recrystallized grains in the forged 0Mn and 0.5Mn alloys is 5.2% and 8.6%, respectively. During the forging process, the alloy is impacted and the as-cast structure is broken, resulting in a large number of dislocations intertwined and knotted to form dislocation cells. With the repeated thickening and stretching of the pier, the storage energy of the alloy is

increased. At the same time, dislocation slip and climb lead to the polygonization, forming a dislocation network with regular arrangement of LAGBs, which leads to the formation of a large number of substructured grains.

2.3 Mechanical properties of as-cast and forged alloys

Fig. 9 shows the engineering stress-engineering strain curves of the as-cast and forged alloys at room temperature and strain rate of $7 \times 10^{-3} \text{ s}^{-1}$. The alloy undergoes two stages of elastic deformation and plastic deformation during the stress process. During the elastic deformation stage, the stress is increased exponentially with the increase in strain. When the loading exceeds the elastic region, the alloy enters the plastic deformation stage, and the stress growth rate is slowed down with the increase in strain, which indicates that there is no obvious work hardening phenomenon in 0Mn and 0.5Mn alloys. When the stress reaches the maximum value, the stress is gradually decreased with the increase in strain until fracture.

The ultimate tensile strength and yield strength of as-cast 0Mn alloy are 882 and 711 MPa, respectively. The elongation and reduction of area are 7.8% and 23.0%, respectively, and the hardness HV is 2881.2 MPa. After adding 0.5wt% Mn, the ultimate tensile strength and yield strength reach 966 and 808 MPa, respectively, and the hardness HV reaches 3194.8 MPa. The mechanical properties of different alloys at different states are shown in Table 2. It can be seen that the hardness and strength of the alloy are increased with the addition of Mn element. However, the elongation and reduction of area decrease to 5.1% and 18.3%, respectively. The Mn addition increases the strength, but the plasticity becomes worse, which may be related to the formation of grain boundary α phase.

Besides, the hardness HV of forged 0Mn alloy is 3175.2 MPa, the ultimate tensile strength and yield strength are 966 and 911 MPa, respectively, and the elongation and reduction of area are 16.4% and 43.8%, respectively. Compared with those of the as-cast 0Mn alloy, the ultimate tensile strength and yield strength increase by 84 and 200 MPa, respectively, and the elongation and reduction of area increase by approximately 2 times. After the forging process, the strength and hardness of the alloy are significantly enhanced, so the forging process is conducive to the improvement in mechanical properties.

After adding 0.5wt% Mn, the hardness HV of the alloy increases to 3361.4 MPa; the ultimate tensile strength and yield strength reach 1079 and 964 MPa, which increase by 113 and 53 MPa compared with those of the forged 0Mn alloy, respectively; the elongation and reduction of area decrease slightly. Compared with those of the as-cast 0.5Mn alloy, the tensile strength and yield strength of the forged 0.5Mn alloy increase by 113 and 156 MPa, respectively; the elongation and reduction of area also increase exponentially.

Fig. 10 shows the tensile fracture morphologies and fracture side morphologies of the as-cast and forged 0Mn and 0.5Mn alloys. Dimples of different sizes and different colors appear in the alloys, which indicates that the alloy produces plastic deformation under the tensile stress during the tensile process and the crack starts in the plastic deformation stage. The dimples are arranged in a network structure. Obvious turning angles and ups and downs can be observed during the crack propagation of the alloys.

According to Fig. 10a, it can be seen that the fracture morphology is accompanied by the cleavage surface, which is

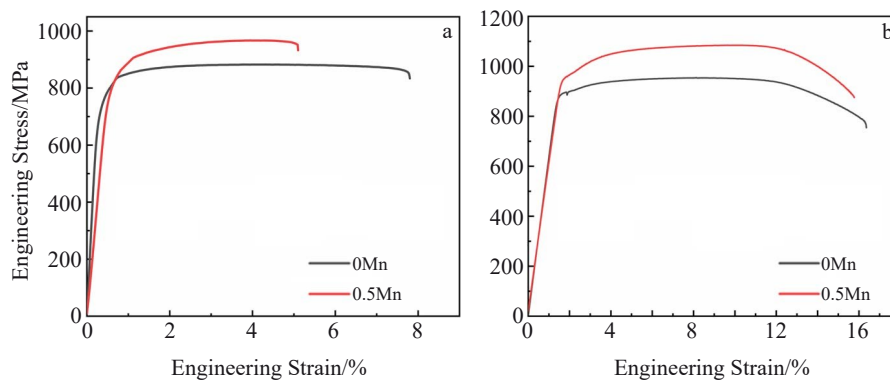


Fig.9 Tensile engineering stress-engineering strain curves of as-cast (a) and forged (b) 0Mn and 0.5Mn alloys

Table 2 Mechanical properties of as-cast and forged 0Mn and 0.5Mn alloys

State	Alloy	Ultimate tensile strength/MPa	Yield strength/MPa	Elongation/%	Reduction of area/%	Hardness, HV/MPa
As-cast	0Mn	882	711	7.8	23.0	2881.2
	0.5Mn	966	808	5.1	18.3	3194.8
Forged	0Mn	966	911	16.4	43.8	3175.2
	0.5Mn	1079	964	15.8	41.3	3361.4

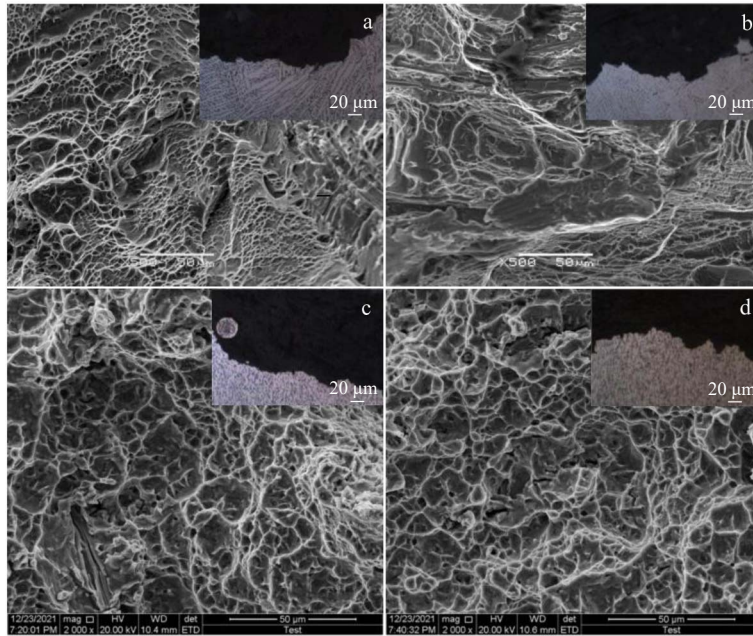


Fig.10 Tensile fracture morphologies and fracture side morphologies of as-cast (a–b) and forged (c–d) 0Mn alloy (a, c) and 0.5Mn alloy (b, d)

similar to rock candy, the dimple size is large, and the color is deep. The dimple is the characteristic of ductile fracture, and the cleavage plane is the characteristic of cleavage fracture, which indicates the brittle fracture. As shown in Fig.10b, it is found that after adding 0.5wt% Mn, the number of dimples in the as-cast 0.5Mn alloy decreases significantly, the color becomes lighter, the size becomes smaller, the number of cleavage planes increases significantly, and the crack propagation becomes more obvious. These phenomena show that there is a certain interaction in the crack propagation process, and it is easier to propagate along the lamellar α phase. The fracture modes of the two alloys show a combination of transgranular fracture and intergranular fracture. Therefore, the fracture mechanism of as-cast 0Mn and 0.5Mn alloys is mixed fracture, and the plasticity of 0Mn alloy is better, which is consistent with the larger elongation of as-cast 0Mn alloy in the tensile test results. A large number of equiaxed dimples are evenly distributed in the fracture morphology of forged 0Mn and 0.5Mn alloys, and the middle area between the large dimples is occupied by small dimples, presenting the typical ductile fracture characteristic. The plastic deformation before fracture is large. The fracture mode of the forged alloy is ductile fracture and microporous aggregation fracture. The direction of crack propagation in the fracture side morphology is in accordance with the direction of micropore aggregation. These phenomena all indicate the transgranular fracture. It is found that the cracks appear near the TiB whiskers and the orientation is unfavorable. This is due to the low bearing capacity of TiB whiskers with low aspect ratio. Thus, the crack is initiated near the boride side.

2.4 Discussion

It is well known that the yield strength of Ti80 alloy

is approximately 800 MPa^[34–35], which is lower than that of TC4 alloy by 20–30 MPa. In this research, the yield strength of forged 0Mn alloy reaches 911 MPa and the good ductility of 16.4% is also obtained. After microalloying with 0.5wt% Mn, the yield strength increases to 964 MPa, the ultimate tensile strength increases significantly, and the ductility slightly decreases to 15.8%. The addition of Mn element as the solute atom causes a certain degree of lattice distortion and increases the resistance against dislocation movement, so the dislocation is difficult to slip, forming a strong solid solution strengthening effect on the alloy and thereby increasing the strength and hardness of the alloy.

The element contents at different locations of 0Mn and 0.5Mn alloys were analyzed by TEM and EDS. The selected points in Fig. 11 are located at the areas at the grain boundaries, near the grain boundaries, and at the α/β phase regions. The content changes of different elements in the alloys are shown in Table 3. Both point 1 and point 2 are located in the β phase, and their Al content is relatively low. Therefore, the average Al content in the β phase of forged 0Mn and 0.5Mn alloys is about 2.15wt% and 2.72wt%, respectively. Mo, Fe, B, and Mn elements are enriched in the β phase. After adding Mn element, Mo is enriched more obviously in the β phase with the average content of about 7.59wt%, which is higher than that in the forged 0Mn alloy by about 2.68wt%. The enrichment of Fe element in the β phase of forged 0Mn alloy is more obvious, and its average content is about 5.81wt%, which is higher than that in the β phase of the forged 0.5Mn alloy by about 1.64wt%. Point 3, 4, and 5 are located in the α phase where Al element is enriched. The Al element in the forged 0.5Mn alloy is higher, and its average content reaches about 7.72wt%, which

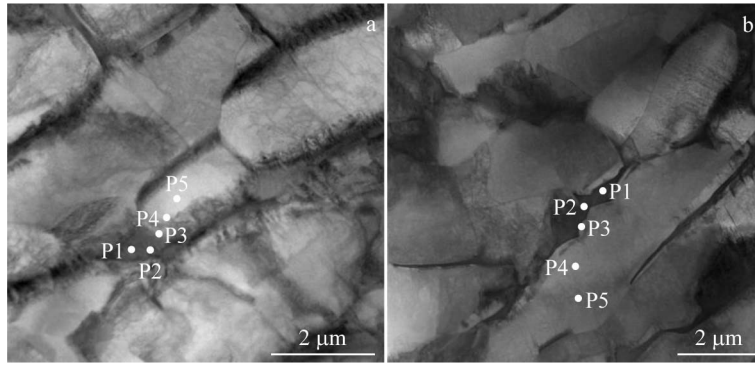


Fig.11 Point selection for EDS element distribution analysis of forged 0Mn alloy (a) and 0.5Mn alloy (b)

Table 3 EDS element contents of selected points in Fig. 11 of forged 0Mn and 0.5Mn alloys (wt%)

Alloy	Point	Ti	Al	Mo	Zr	Fe	B	Mn
0Mn	1	84.65	2.11	4.79	1.33	5.22	1.86	0.00
	2	81.63	2.19	5.03	2.15	6.40	2.57	0.00
	3	90.80	5.62	0.00	2.30	0.38	0.87	0.00
	4	90.89	5.46	1.11	0.96	0.26	1.28	0.00
	5	90.72	6.47	0.00	1.23	0.29	1.26	0.00
0.5Mn	1	78.42	2.85	8.14	1.01	4.18	2.79	2.58
	2	76.84	2.58	7.03	2.53	4.16	3.35	3.47
	3	89.01	6.57	1.98	1.23	0.21	0.84	2.13
	4	89.08	8.03	1.08	0.56	0.06	0.38	0.78
	5	87.54	8.56	1.13	0.88	0.06	1.21	0.57

is higher than that in the α phase of forged 0Mn alloy by 1.87wt%.

According to EDS test results, the Mn element is enriched at the grain boundary and in the β phase. From the thermodynamic analysis, when the alloying element Mn accumulates at the grain boundary in the form of impurity atoms or solid solution, it will have a drag effect on the grain boundary, resulting in the decrease in grain boundary energy. The Mn enrichment will also reduce the driving force of grain growth and refine the grains, which is beneficial to the strength and plasticity of the alloy. From the kinetic analysis, the enrichment of Mn element at the grain boundary will exert a pinning effect on the grain boundary, hinder the movement of the grain boundary, reduce the grain boundary mobility, and thus improve the strength of the alloy^[36-37]. At the same time, Mn element is a eutectoid β stable element, and the addition of Mn will increase the content of β phase, resulting in more grain boundaries to hinder the dislocation movement^[38].

Furthermore, the addition of Mn element results in the dissolution of more Al atoms into the α phase, whereas the Mo atoms are more concentrated in the β phase. The solid

solution strengthening effect of β -stable elements in the β phase is quite weak. Even if the β matrix has plenty β -stable elements, such as Mo, the hardness increment of β phase is still very limited. The hardness of the primary α phase is affected by the solid solution strengthening of Al element, and it is increased with the increase in the solid solution Al content. The solid solution of Al and Mn elements will increase the dislocation slip resistance. Al solute can effectively reduce the basal stacking fault energy and adjust the binding energy difference between different slip systems and that between hcp and face-centered cubic phases, which is more conducive to the plane slip^[36,39-40]. The inhomogeneity of microstructure will inevitably lead to the division of stress and strain between the soft and hard regions inside the alloy, resulting in the reverse stress in the soft region to offset the applied stress and leading to the positive stress in the hard region to promote the deformation. Consequently, the synergistic strengthening effect is enhanced and the alloy strength is improved^[41].

In addition, the 0.5wt% Mn addition is beneficial to the refinement of lamellar α phase in the as-cast alloy, and results in the more equiaxed and homogeneous microstructure after subsequent forging process. The 0.5Mn alloy possesses more recrystallized grains and HAGBs. When the dislocation slips through the grain boundary, the deformation energy can be quickly dispersed into each grain to reduce the dislocation pile-up phenomenon, and the stress concentration at the grain boundary is small, which is beneficial to the plasticity retainment.

3 Conclusions

1) The addition of Mn element can refine the thickness of lamellar α phase in the as-cast Ti-Al-Mo-Zr-Fe-B alloy, and the average thickness decreases from 3.28 μm to 2.65 μm after 0.5wt% Mn addition. After forging process, the average grain sizes of the two alloys are similar. The grains of forged 0.5Mn alloy tend to be more equiaxed and homogeneous.

2) The strength and hardness of the titanium alloys are significantly enhanced by Mn microalloying. After adding 0.5wt% Mn, the ultimate tensile strength and yield strength of forged alloy reach 1079 and 964 MPa, respectively, and good

ductility of 15.8% is also obtained.

3) The addition of Mn element has a certain solid strengthening effect and promotes the enrichment of Al element in the α phase, which cannot only reduce the stacking fault energy of the alloy, but also improve the hardness of α phase, resulting in the synergistic strengthening effect caused by the uneven hardness of different phases in the alloy. Thus, the strength is improved and the good plasticity can be retained.

References

- Banerjee D, Williams J C. *Acta Materialia*[J], 2013, 61(3): 844
- Sun Y Y, Chen K, Alexandrov I V et al. *International Journal of Fatigue*[J], 2023, 169: 107497
- Meng K, Guo K, Yu Q et al. *Corrosion Science*[J], 2021, 183: 109320
- Wang Q, Ren J Q, Wu Y K et al. *Journal of Alloys and Compounds*[J], 2019, 789: 249
- Niu J Z, Dai G Q, Guo Y H et al. *Composites Part B: Engineering*[J], 2021, 216: 108854
- Yue D Z, Jiang X Z, Yu H Y et al. *Chemical Engineering Journal*[J], 2023, 463: 142389
- Yang Qi, Hui Songxiao, Ye Wenjun et al. *Rare Metal Materials and Engineering*[J], 2023, 52(3): 899 (in Chinese)
- Wang B, Zhou L, Cao Y S et al. *Journal of Materials Research and Technology*[J], 2023, 24: 7462
- Guan H T, Fu Q, Xiang W et al. *Materials Research Express*[J], 2023, 10(4): 046503
- Xiong J H, Li S K, Gao F Y et al. *Materials Science and Engineering A*[J], 2015, 640: 419
- Gao F Y, Gao Q, Jiang P et al. *International Journal of Lightweight Materials and Manufacture*[J], 2018, 1(4): 265
- Ren J Q, Wang Q, Zhang B B et al. *Materials Science and Engineering A*[J], 2022, 831: 142187
- Ren J Q, Wang Q, Zhang B B et al. *Intermetallics*[J], 2021, 130: 107058
- Guo Y H, Liu G, Jiao T Z et al. *International Journal of Mechanical Sciences*[J], 2023, 245: 108135
- Su B X, Wang B B, Luo L S et al. *Journal of Materials Science and Technology*[J], 2021, 74: 143
- Liu Shun, Xu Mang, Li Tianrui et al. *Rare Metal Materials and Engineering*[J], 2021, 50(9): 3203 (in Chinese)
- Wang Qiming, Yang Jing, Chen Haisheng et al. *Titanium Industry Progress*[J], 2023, 40(5): 9 (in Chinese)
- Yan C, Wang C, He M X et al. *Crystals*[J], 2022, 12(11): 1584
- Dai G Q, Niu J Z, Guo Y H et al. *Journal of Materials Research and Technology*[J], 2021, 15: 1881
- Cui X F, Mi X J, Luo Z et al. *Journal of Materials Engineering and Performance*[J], 2014, 24(1): 67
- Ouyang Delai, Xie Youmei, Hu Shengwei et al. *Rare Metal Materials and Engineering*[J], 2023, 52(2): 710 (in Chinese)
- Wang Weizhen, Zhou Xinzhe, Yang Zhiqing et al. *Materials China*[J], 2023, 42(3): 185 (in Chinese)
- Ju J T, Wang Y, Hao F et al. *Rare Metal Materials and Engineering*[J], 2019, 48(6): 1749
- Jiang Tao, Hu Renmin, Zhu Kailiang et al. *China Science-paper*[J], 2014, 9(8): 944 (in Chinese)
- Moiseyev V N. *Titanium Alloys: Russian Aircraft and Aerospace Applications*[M]. Dong Baoming, Trans. Beijing: Aviation Industry Press, 2008: 19 (in Chinese)
- Zhang F M, Weidmann A, Nebe J B et al. *Journal of Biomedical Materials Research Part B: Applied Biomaterials*[J], 2010, 94B(2): 406
- Jawed S F, Rabadia C D, Liu Y J et al. *Materials Science and Engineering C*[J], 2020, 110: 110728
- Liu J, Luan Q D, Wang X G et al. *Materials Science and Engineering A*[J], 2010, 527(29–30): 7658
- Liu Ji Yao, Wang Wenyan, Huang Yabo et al. *Heat Treatment of Metals*[J], 2017, 42(8): 89 (in Chinese)
- Sun Y Y, Alexandrov I V, Dong Y C et al. *Journal of Materials Research and Technology*[J], 2021, 15: 5277
- Chen Z, Liu Y, Jiang H et al. *Journal of Alloys and Compounds*[J], 2017, 723: 1091
- Hémery S, Nait-Ali A, Guéguen M et al. *Materials & Design*[J], 2018, 137: 22
- Aguilar C, Aguirre T, Martínez C et al. *Materials & Design*[J], 2020, 195: 108945
- Luo G L, Zhang L F, Xiong Y et al. *Journal of Materials Engineering and Performance*[J], 2022, 31(7): 5571
- Hua Yao. *Heat Treatment of Metals*[J], 2021, 46(9): 146 (in Chinese)
- Niu R M, An X H, Li L L et al. *Acta Materialia*[J], 2022, 223: 117460
- Zhao B K, Huang P, Zhang L B et al. *Scientific Reports*[J], 2020, 10(1): 3086
- Huang Qingguo, Ying Zixiang, Wang Zhilei et al. *Rare Metal Materials and Engineering*[J], 2024, 53(3): 718 (in Chinese)
- Qin D Y, Lu Y F, Guo D Z et al. *Materials Science and Engineering A*[J], 2013, 587: 100
- Wei B Q, Wu W Q, Gong M Y et al. *Acta Materialia*[J], 2023, 245: 118637
- Zhu Y T, Wu X L. *Materials Research Letters*[J], 2019, 7(10): 393

Mn 微合金化对 Ti-Al-Mo-Zr-Fe-B 合金组织演变和力学性能的影响

何苗霞¹, 燕 迟², 董月成¹, 常 辉¹, Alexandrov Igor V²

(1. 南京工业大学 材料科学与工程学院 新材料研究院, 江苏 南京 211816)

(2. 乌法理工大学 材料科学与金属物理系, 俄罗斯 乌法 450008)

摘 要: 通过 OM、EBSD 和 TEM 等研究了 Mn 微合金化对新型近 α Ti-Al-Mo-Zr-Fe-B 合金微观组织和力学性能的影响。结果表明: 添加 0.5% (质量分数) 的 Mn 元素可以将合金的铸态微观组织从 3.28 μm 细化到 2.65 μm , 使其抗拉伸强度从 882 MPa 提高到 966 MPa, 但延伸率从 7.8% 下降到 5.1%。锻造后的 2 种合金的晶粒尺寸趋于一致, 微观组织趋于等轴化且 Mn 微合金化后的组织更加均匀。锻造后, Ti-Al-Mo-Zr-Fe-B 合金的抗拉伸强度和延伸率增加到 966 MPa 和 16.4%, 而含有 0.5% (质量分数) Mn 元素的合金具有更高的抗拉伸强度, 达到了 1079 MPa, 同时延伸率达到了 15.8%。结论表明, 强度的提高可以归因于 Mn 元素的固溶强化效应, 同时 Mn 微合金化处理使合金中的 Al 元素富集于 α 相, 有利于提高合金的强度和塑性。

关键词: Mn 微合金化; 近 α 钛合金; 组织演变; 力学性能

作者简介: 何苗霞, 女, 1997 年生, 硕士生, 南京工业大学材料科学与工程学院新材料研究院, 江苏 南京 211816, E-mail: mxhesy1018@njtech.edu.cn